J.K.N. Tan, A.W. Law, A.K. Maan and S.H. Cheung (2023). Digital-twin-controlled ventilation for real-time resilience against transmission of airborne infectious disease in an indoor food court. *Building Services Engineering Research & Technology*.

https://doi.org/10.1177/01436244231204450

Published in Oct. 2023

Digital-twin-controlled ventilation for real-time resilience against transmission of airborne infectious disease in an indoor food court

Jonathan Koon Ngee TAN[a,b], Adrian Wing-Keung LAW[b,c*], Akshay Kumar MAAN[a,b], Sai Hung CHEUNG[d]

[a] *Institute of Catastrophe Risk Management, Nanyang Technological University, 50 Nanyang Avenue, Singapore 639798*

[b] *Future Resilient Systems, Singapore-ETH Centre, 1 Create Way, Singapore 138602*

[c] *School of Civil and Environmental Engineering, Nanyang Technological University, 50 Nanyang Avenue, Singapore 6397983*

[d] *Department of Civil Engineering, the University of Hong Kong, Pokfulam Road, Hong Kong*

** Corresponding author*

Email address: cwklaw@ntu.edu.sg

Abstract

The needs of a physical system evolve throughout a disruption event. Therefore, responses to mitigate a disruption should be recalibrated in a timely manner to target the current needs of the disrupted system. The concept of real-time resilience is defined, which encapsulates the capacity of a system to continuously recalibrate its responses to a disruption. In this study, metrics to

quantify the added value of having such resilience are proposed. As a case study of real-time resilience, the resilience against airborne disease transmission in an indoor food court with digital-twin-controlled ventilation was investigated, and the application of the metrics for evaluating the resilience enhancements enabled by the dynamic response strategy of the ventilation system was demonstrated. Comparative simulations showed that higher adaptive capacities in a mixing ventilation system enhanced the overall resilience of the diners in terms of percentage improvements to the disruption duration (26%–61%), loss of resilience (2%–39%), and average rate of recovery (26%–74%). At the same time, the tempo-spatial trends of individual resilience suggested that increasing the ventilation rate could simultaneously increase the dilution and dispersion of infectious aerosols, which had opposing effects on resilience. The overall effect would depend on the specific locations of the diners. Based on the results, the tradeoff between resilience and energy use was also discussed.

Keywords

Real-time resilience, dynamic response strategy, airborne infectious disease, digital-twin-controlled ventilation

1. Introduction

As a disruption event unfolds in a system, the states of both the disruption and the disrupted system evolve continuously. The responses enacted to mitigate the disruption should, therefore, be recalibrated in a timely manner to meet the current needs of the system. However, there is a paucity of research regarding such recalibration for resilience. Building on the concept of resilience (Hollnagel et al., 2006), we define real-time resilience as the capacity of a system to respond to

disruptions in a dynamic manner involving continuous recalibration of its resisting, adapting, and recovering actions, based on real-time information of the evolving states of both the disruption and the system. The concept of responses based on real-time information is not new in the resilience literature. It has been discussed for disruptions and systems of different natures and scales, for example, stealthy sensor attacks on cyber-physical systems (Kim et al., 2021), natural disasters damaging distribution systems (Lei et al., 2016), and unfavorable rainfall impacting agricultural systems (Boyd et al., 2013). Real-time resilience extends this concept by encapsulating the ability of the system to continuously learn from historical and new information to improve responses. Building real-time resilience in systems confers two advantages. Firstly, it enables the responses to become more effective over time as decision makers receive real-time information regarding the disruptions and systems which can be analyzed to obtain insights for improvements. Secondly, it enables timelier predictive responses to be made given the continuous monitoring of the relevant entities which facilitates the detection of early stages of disruptions. Hence, the responses are likely more efficient and the scale of the damage and the chances of cascading failures in the disrupted system are reduced (Noebels et al., 2022).

In order to achieve real-time resilience, a dynamic response strategy needs to be developed that is comparable to adaptive control but more advanced with an objective of mitigating disruptions defined by specific metrics. The strategy would also involve repeated decision making in set time intervals. At each time interval, the strategy can be broken down into three steps. The first step is sensing which is the process of observing or estimating the current states of the disrupted system and the disruption. This step is a prerequisite for designing, initiating, and implementing effective and efficient responses to mitigate the disruption. The next step is sensemaking which is defined here as the process of analyzing the sensed data, typically in the

context of historic information and what-if scenarios, to obtain insights about the causes, effects, and possible trajectories of the current states of system and disruption. The final step is recalibration where the current response is adjusted or replaced with an alternative according to the insights gained from sensemaking coupled with optimization procedures, precomputed rules, and/or heuristics. Correspondingly, real-time resilience requires the adequate sensorization of the systems, establishment of bidirectional flows of real-time information between the systems and decision makers, and building of models and simulations that are capable of real-time sensemaking and recalibration.

A rising enabler for real-time resilience is the digital twin technology which encapsulates the intersection of computational power, sensors, Internet of Things, big data analytics, modelling, and simulations (Tao et al., 2019). A digital twin is a virtual representation of a physical entity that is constantly mimicking the current state of the entity (Rasheed et al., 2019). It can provide real-time monitoring, anomaly detection, root-cause identification, impact assessment, and what-if analyses to support timely decision making (Eirinakis et al., 2022). Consequently, it is well suited for implementing dynamic response strategies, and had been applied for resilience building in cyber-physical systems (Flammini, 2021; Saad et al., 2020), critical infrastructures (Brucherseifer et al., 2021), and manufacturing (Bécue et al., 2020; Burgos and Ivanov, 2021). While studies have proposed conceptual frameworks and demonstrated implementations of digital twins for real-time resilience, the research questions of "In what ways can digital twins affect real-time resilience and by how much?" and "Does the added value of real-time resilience justify the costs of adopting digital twins as an enabler?" remain largely unexplored. The aims of this paper are to address the above research gaps in the following manner: 1) propose metrics to quantify the value of real-time resilience, 2) demonstrate the application of the proposed metrics for evaluating the effectiveness

of a dynamic response strategy for disruption mitigation through a novel case study of resilience against airborne disease transmission in an indoor environment with a digital-twin-controlled ventilation system, and 3) investigate the tradeoff between resilience and energy use in the case study.

The paper is organized as follows. In Section 2, we present the quantitative metrics to evaluate real-time resilience which can be generalized to any systems and disruptions. Section 3 describes the case study, covering the systems and ventilation scenarios investigated in detail, as well as the comparative simulations and analyses of resilience and energy use. Section 4 focuses on the computational results. In Section 5, we discuss the implications of the results to the research questions within the context of the case study and draw some lessons to enhance real-time resilience in physical systems. Finally, we conclude in Section 6 by summarizing the paper's main contributions and highlighting areas for future research.

2. Real-time resilience metrics

Resilience metrics of a system can be deconstructed as measures of the magnitude and duration of the fluctuations in system performance following a disruption. For any system, a robustness range can be defined to describe the limits for acceptable levels of performance (Tang and Heinimann, 2019). In a general system resilience curve (Figure 1), t_{ds} and t_{df} are the times at which the performance level first drops below and rises above the lower bound of the robustness range R_l, respectively, after the occurrence of a disruption, $P_v(t)$ is the minimum performance level observed between t_{ds} and time instance t, with $P_v(t_{df})$ corresponding to the level exhibited by the system in the vulnerable phase, and P_o is the original performance level which is assumed to be the ideal level for the system. From this curve, the resilience metrics that can be computed

include the disruption duration T_d which is the length of time during which the performance is out of the robustness range, the impact $r(t)$ which represents the magnitude of the maximum decline in performance between t_{ds} and t, the loss of resilience $\Psi_{loss}(t)$ which represents the overall performance loss from t_{ds} to t that can be quantified by the area bounded by the resilience curve and R_l during this time period, and the instantaneous rates of degradation $\nabla P_D(t)$ and recovery $\nabla P_R(t)$ (Yodo and Wang, 2016). For t in the range of t_{ds} and t_{df}, these resilience metrics can be evaluated as:

$$T_d = t_{df} - t_{ds} \tag{1}$$

$$r(t) = R_l - P_v(t) \tag{2}$$

$$\Psi_{loss}(t) = \int_{t_{ds}}^{t} [R_l - P(t')]dt' \tag{3}$$

$$\nabla P_D(t) = -\frac{dP_D}{dt'}\Big|_{t'=t} \tag{4}$$

$$\nabla P_R(t) = \frac{dP_R}{dt'}\Big|_{t'=t} \tag{5}$$

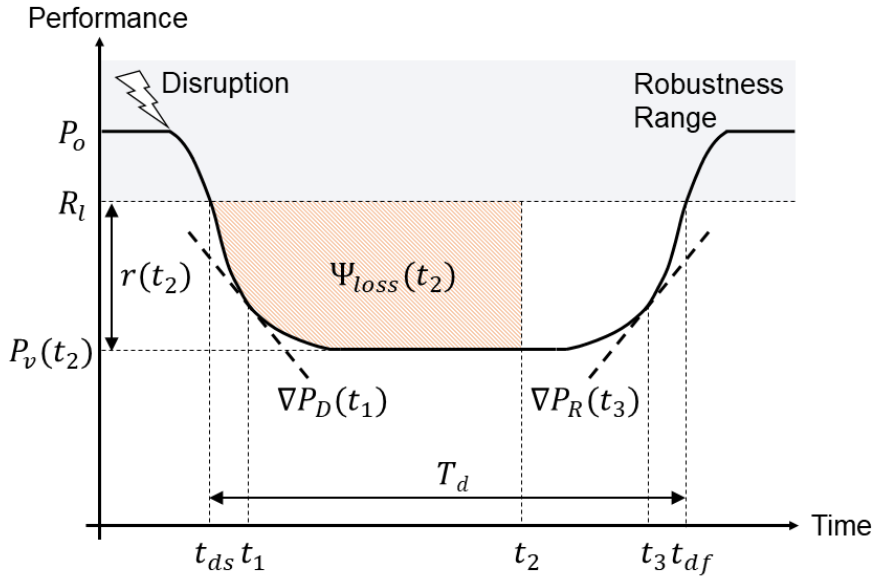

Fig. 1 General resilience curve showing the resilience metrics of disruption duration T_d, impact $r(t)$ and loss of resilience $\Psi_{loss}(t)$ at arbitrarily chosen time instance t_2, and instantaneous rates of degradation $\nabla P_D(t)$ and recovery $\nabla P_R(t)$ at arbitrarily chosen times t_1 and t_3, respectively.

A system with real-time resilience can analyze information about the current level of its performance in the context of fault tolerance thresholds such as the robustness range as well as historical and predicted trajectories of performance to obtain insights for recalibrating its mitigation responses to the disruption. As illustrated in Figure 2, a system with such capacity can continuously improve its resisting and recovering actions throughout the disruption event. Given that $\nabla P_D(t)$ and $\nabla P_R(t)$ of a system with real-time resilience change every time the response is recalibrated, the average rates of degradation and recovery during the period of t_{ds} to t, $\overline{\nabla P_D}(t)$ and $\overline{\nabla P_R}(t)$, can be computed as resilience metrics for comparison. To quantify the added value of real-time resilience, the percentage improvements in T_d, $r(t)$, $\Psi_{loss}(t)$, $\overline{\nabla P_D}(t)$ and $\overline{\nabla P_R}(t)$ between the same system with and without the resilience can be computed as:

$$\frac{x(e_b - e_{rt})}{e_b} \times 100\% \tag{6}$$

$$x = \begin{cases} 1 \; if \; e \in \{\mathrm{T}_d, r(t), \Psi_{loss}(t), \overline{\nabla P_D}(t)\} \\ -1 \; if \; e \in \{\overline{\nabla P_R}(t)\} \end{cases} \tag{7}$$

where e is the resilience metric of interest and the subscripts rt and b refer to the system with real-time resilience and without it, respectively. Having real-time resilience also confers systems the ability to monitor their resilience metrics over time, which is rarely done in conventional resilience analyses.

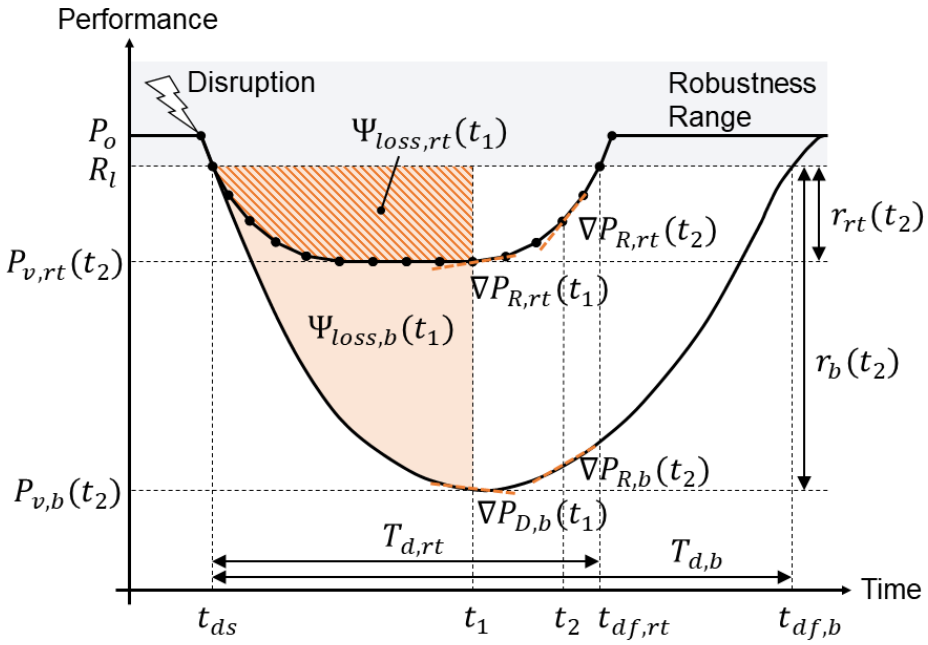

Fig. 2 Resilience curves for system with and without real-time resilience, as indicated by the subscripts rt and b, respectively. The added value of having real-time resilience can be measured by the percentage improvements in the resilience metrics, disruption duration T_d and impact $r(t)$ and loss of resilience $\Psi_{loss}(t)$ at the time instances of interest. The average rates of degradation and recovery, $\overline{\nabla P_D}(t)$ and $\overline{\nabla P_R}(t)$, can be computed from the instantaneous rates such as those shown in the figure and compared like the other resilience metrics.

3. A case study of real-time resilience: transmission of airborne infectious disease in an indoor air-conditioned food court

3.1. Definitions of disruption, system, and resilience for the case study

The purpose of the case study is to illustrate how real-time resilience can be enabled and assessed in a realistic setting. This section defines the disruption, system, and resilience investigated in the case study. In the setting of an indoor air-conditioned food court, the disruption event of interest is the occurrence of a diner infected with an airborne disease exhaling infectious aerosols during his or her dwell duration. COVID-19 was selected as the airborne infectious disease for the current investigation given its global prevalence and impact in recent years. An indoor food court, also known as a food hall or cafeteria, was chosen as the setting representing a

ubiquitous indoor space use where congregations of unmasked people are guaranteed. Moreover, the seat turnover rate in food courts can be high enough such that many different individuals use the spaces during meal times, yet their respective seating durations are long enough for their exposure to infectious aerosols to reach unsafe levels should there be an infectious diner within their vicinity. Correspondingly, the system investigated includes the air volume within the food court and the mechanical ventilation system serving the space which provides a means to respond to the disruption by controlling the amount of clean air supplied to the diners. The measure of performance for the system is the diner's probability of getting infected, herein termed as the individual infection risk P_I.

Based on the disruption and system defined above, the resilience of the diners against COVID-19 infection can be derived from the plots of their respective infection risks over time (Figure 3). These infection risk curves can be viewed as resilience curves that are inverted along the horizontal axis, with a safety threshold P_{ST} being the equivalent to the lower bound of the robustness range of an engineering system and acceptable 'system performance' defined as P_I being lower than P_{ST}. While there is no clear consensus thus far on the appropriate value of P_{ST}, for the purposes of this illustrative example, P_{ST} is taken to be 10^{-3} (Buonanno et al., 2020) which is obtained by comparing the mortality rates of COVID-19 with those of carcinogenic diseases which have a defined value for unacceptable risks (Toner, 2008). As described in Section 2, the resilience of the diners can be evaluated using T_d, the total amount of time where P_I is not acceptable, i.e., exceeds P_{ST}, $r(t)$, the maximum P_I experienced in a specified dwell period, $\Psi_{loss}(t)$, a measure of the overall exposure to infection risks throughout the dwell period of interest, as quantified by the area below the infection risk curve that exceeds P_{ST} (shaded area in

Figure 3), and the average rates of degradation $\overline{\nabla P_D}(t)$ and recovery $\overline{\nabla P_R}(t)$ during the dwell period.

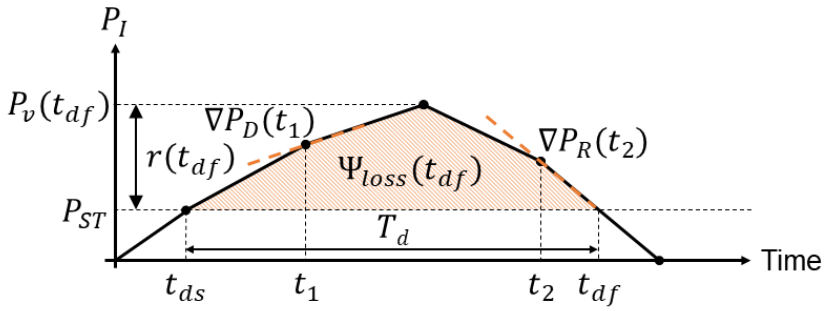

Fig 3. Example of a resilience curve of individual infection risk P_I against time. The resilience metrics of disruption duration T_d, impact $r(t)$ and loss of resilience $\Psi_{loss}(t)$ considering the entire T_d, and instantaneous rates of degradation $\nabla P_D(t)$ and recovery $\nabla P_R(t)$ at selected times are illustrated. P_{ST} is the safety threshold for infection risk.

3.2. Indoor air-conditioned food court

The design of the food court simulated for this illustrative example is adapted from the study site of Chitaru et al (Chitaru et al., 2018) which is a mechanically ventilated cafeteria in Constanta, Romania. The food court has dimensions of 26.5 m × 11.25 m × 3.2 m (length × width × height) with an opening of size 4 m × 2 m that serves as the entrance and exit of the enclosed area (Figure 5). On the ceiling, there are eight air supply vents with dimensions of 0.5 m × 0.43 m and three circle-shaped return air vents with diameters of 0.8 m which are part of a conventional mixing type ventilation system. The indoor space contains ten tables and 40 chairs.

3.3. Digital-twin-controlled mechanical ventilation as an enabler of real-time resilience

To enable real-time recalibration of ventilation based on the estimated P_I, the mixing ventilation system for the food court is coupled with a digital-twin control comprising of four modules with distinct functions, namely, occupancy detection, aerosol dispersion simulation,

infection risk estimation, and ventilation rate control (Figure 4). The digital-twin control provides the ventilation system with the capacity to implement a dynamic response strategy against transmission of COVID-19, with the first module providing sensing capacity, the next two modules providing sensemaking capacity, and the last module providing recalibration capacity. Overall, the dynamic strategy implemented is an iterative process where P_I assessment and mitigation are executed repeatedly at regular time intervals, herein termed as control intervals, throughout the operation of the ventilation system. In the context of this digital-twin control, P_I refers to the infection risk of an individual owing to his or her exposure to infectious aerosols over a control interval.

3.3.1. Occupancy detector

The diners, being infectious or susceptible individuals, are the sources and sinks, respectively, of the infectious aerosols in the space. Hence, it is imperative to regularly sense the current location of each diner (x_i, y_i, z_i) where i refers to the ith diner. This sensing step is implemented at the start of each control interval and could be achieved using cameras or chair sensors for the food court setting. It is assumed that the diners are stationary in their detected coordinates during the control interval.

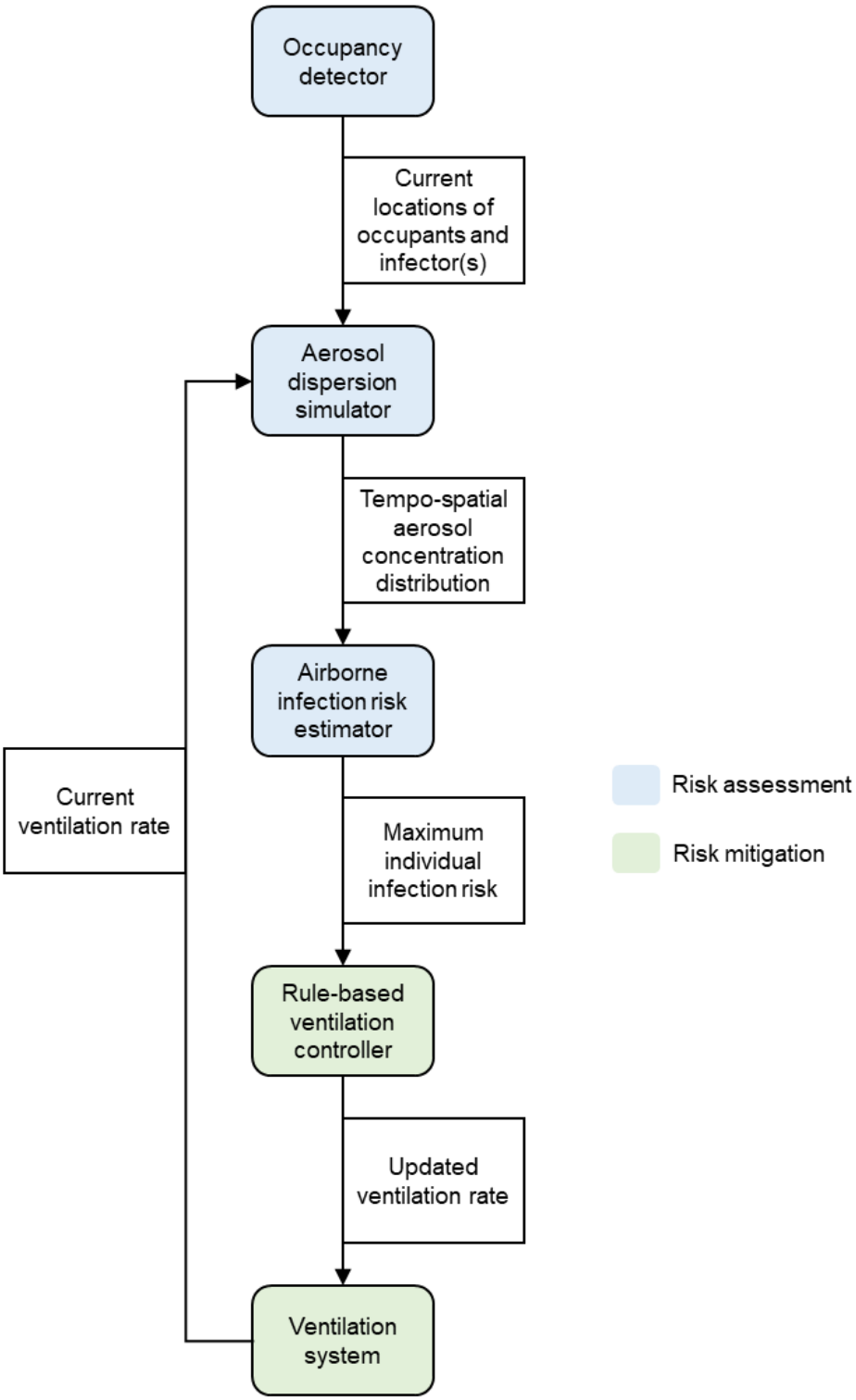

Fig 4. Flowchart of the processes occurring in one control interval under the dynamic response strategy implemented by the digital-twin control of the ventilation system

3.3.2. Aerosol dispersion simulator

The second module of the digital-twin control is an ongoing transient computational fluid dynamics (CFD) simulation of the indoor air and the tempo-spatial transport of infectious aerosols in the food court. Simulations of the physical entity of interest is a defining characteristic of digital twins and their predictive abilities are utilized by the control in this case study for sensemaking. Importantly, the simulation is updated at the start of each control interval based on the sensed data about the current locations of the diners (x_i, y_i, z_i) and the current hour rate of the ventilation system V_h (m^3/h). While simulating the system within the duration of a control interval, the module exports data of the molar concentration of infectious aerosols, recorded every five seconds during the control interval, to the subsequent module for the estimation of P_I. In the simulation, each identified infectious diner is modelled as an emission source of infectious aerosols, with exhaled water vapor used as a proxy for the emitted virus-laden aerosols (Ho, 2021; Ho and Binns, 2021). The mass emission rate of water vapor from an infectious diner, MER (kg/h), can be evaluated as:

$$MER = ER \cdot V_d \cdot \rho_w \tag{8}$$

where ER (m^3/h) is the exhalation rate, V_d (mL/m^3) is the droplet volume concentration emitted by the infectious diner, and ρ_w (kg/mL) is the density of water. ER of an infectious diner is taken to be 1.38 m^3/h, a representative value for a speaking person in an indoor space (Buonanno et al., 2020). The inhalation rate, IR, of a susceptible diner is assumed to be 1.38 m^3/h. V_d is assumed to be 6×10^{-2} mL/m^3 which is a conservative value (Buonanno et al., 2020) estimated by dividing the average droplet volume emission rate of a loud speaking individual (Stadnytskyi et al., 2020) by his or her expiration rate for standing activity (Adams, 1993). The Eulerian approach is taken for the CFD simulation and the conservation equations for mass and momentum can be expressed, respectively, as (ANSYS, Inc., 2021):

$$\frac{\partial \rho}{\partial t} + \nabla \cdot (\rho \vec{v}) = S_m \tag{9}$$

$$\frac{\partial}{\partial t}(\rho \vec{v}) + \nabla \cdot (\rho \vec{v} \otimes \vec{v}) = -\nabla p + \nabla \cdot (\bar{\bar{\tau}}) + \rho \vec{g} \tag{10}$$

where ρ is the density of the fluid, $\vec{v}$ is the velocity vector, S_m is the mass source term for the gas mixture in the food court, p is the static pressure, $\vec{g}$ is the gravitational acceleration vector, and $\bar{\bar{\tau}}$ is the fluid viscous stress tensor which is given by:

$$\bar{\bar{\tau}} = \mu[(\nabla \vec{v} + \nabla \vec{v}^T) - \frac{2}{3} \nabla \cdot \vec{v} I] \tag{11}$$

where μ is the molecular viscosity and I is the unit tensor. An energy equation in the following form is also solved (ANSYS, Inc., 2021):

$$\frac{\partial}{\partial x}(\rho E) + \nabla \cdot [\vec{v}(\rho E + p)] = \nabla \cdot (k_{eff} \nabla T - \sum_i h_i \vec{J}_i) \tag{12}$$

where k_{eff} is the effective conductivity, T is temperature, h_i is the sensible heat of species i, $\vec{J}_i$ is the diffusion flux of species i, and E is defined as:

$$E = \mathrm{h} - \frac{p}{\rho} + \frac{v^2}{2} \tag{13}$$

where h is enthalpy and v is fluid velocity. The SST k-omega viscous model and species transport model(ANSYS, Inc., 2021) are employed to model the transient dispersion of infectious aerosols. The transport equations for the turbulence kinetic energy, k, and the specific dissipation rate, ω, for the k-omega model are expressed, respectively, as:

$$\frac{\partial}{\partial t}(\rho k) + \frac{\partial}{\partial x_i}(\rho k u_i) = \frac{\partial}{\partial x_j}\left(\Gamma_k \frac{\partial k}{\partial x_j}\right) + G_k - Y_k + G_b \tag{14}$$

$$\frac{\partial}{\partial t}(\rho \omega) + \frac{\partial}{\partial x_i}(\rho \omega u_i) = \frac{\partial}{\partial x_j}\left(\Gamma_\omega \frac{\partial \omega}{\partial x_j}\right) + G_\omega - Y_\omega + D_\omega + G_{\omega b} \tag{15}$$

where G_k is the production of turbulence kinetic energy due to mean velocity gradients, G_ω is the generation of ω, Γ_k and Γ_ω are the effective diffusivity of k and ω, respectively, Y_k and Y_ω are the dissipation of k and ω due to turbulence, respectively, D_ω is the cross-diffusion term, and G_b and

$G_{\omega b}$ are the buoyancy source terms for k and ω, respectively. The conservation equation for each species in the mixture is:

$$\frac{\partial}{\partial t}(\rho Y_i) + \nabla \cdot (\rho \vec{v} Y_i) = -\nabla \cdot \vec{J}_i + S_m \tag{16}$$

where Y_i is the local mass fraction of species i, S_m is the emission of water vapor from all the infectors in the space at the rate defined in equation 1 and it is equal to zero for all the other species of gases in the mixture, and $\vec{J}_i$ is the mass diffusion flux of species i which can be evaluated as:

$$\vec{J}_i = -\left(\rho D_{i,m} + \frac{\mu_t}{Sc_t}\right)\nabla Y_i - D_{T,i}\frac{\nabla T}{T} \tag{17}$$

where $D_{i,m}$ is the mass diffusion coefficient for species i, μ_t is the turbulent viscosity, Sc_t is the turbulent Schmidt number, and $D_{T,i}$ is the thermal diffusion coefficient for species i.

For this illustrative example, a 3D model of the food court is built in SpaceClaim and the volume of indoor air is imported into ANSYS 2021 R1 Fluent as a mesh with 2,575,110 cells for numerical simulation. To verify the mesh sensitivity, time-averaged air velocities at the breathing zones of three diners, located at seats 4 (near the entrance), 22 (middle), and 40 (far from the entrance), respectively, were compared across three mesh resolutions (1,591,908, 2,575,110, and 3,790,954). The sizing of the cells in the coarsest and intermediate resolutions are three times and 1.5 times that of the finest resolution, respectively. The breathing zone of a diner is demarcated as a cubical volume with length of 0.4 m and a centre of origin at the point 5 mm in front of the centre of the face of the diner (Figure 5). The velocities considered for the mesh sensitivity analysis were obtained from the period of 0s to 3600s during the initialization simulation which represents the practice of purging the indoor air with a ventilation rate of 2405 m^3/h, i.e., 10 L/s/person assuming maximum occupancy of 40 diners, for one hour before occupancy. As shown in Table 1, the relative difference between the intermediate and finest mesh are approximately equal to or less than 5% and thus, it is estimated that a mesh resolution of 2,575,110 is accurate enough. The

boundary conditions for the walls, the air supply vents, and the return air vents as well as the opening to the enclosed space are defined as no slip walls, velocity inlets, and pressure outlets with zero gage pressure, respectively. The indoor and outdoor temperatures are set as 20°C and 27°C, respectively, reflecting conditions in a warm season or climate. Seated diners are represented by simplified human models in the mesh (Figure 5).

Table 1. Relative differences of the time-averaged air velocities at the breathing zones of the diners at seats 4 (near the entrance), 22 (middle of the food court), and 40 (far from the entrance) across the meshes with coarsest (1,591,908 cells), intermediate (2,575,110 cells), and finest (3,790,954 cells) resolution.

Seat	Relative difference between coarsest and intermediate mesh (%)	Relative difference between intermediate and finest mesh (%)
4	10.1	5.3
22	12.1	5.1
40	2.2	1.1

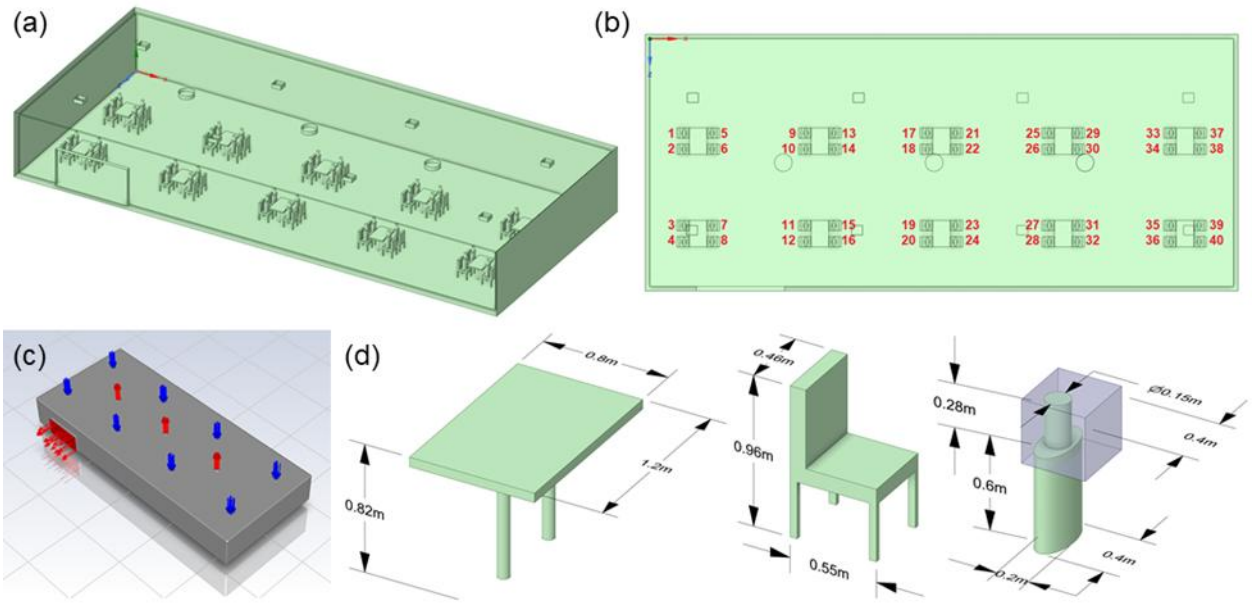

Fig 5. Details of the indoor food court model. (a) Trimetric view of the model with the indoor space shown. (b) Top-down view of the space with the seat numbers shown. (c) Model with the airflow into the space visualized by blue arrows and airflow out visualized by red arrows. (d) Dimensions of the tables, chairs, human models, and breathing zone of each diner.

3.3.3. Airborne infection risk estimator

This module computes P_I of the diners using an infection risk model (Buonanno et al., 2020) modified to incorporate the tempo-spatial variations of the concentration of the infectious aerosols in the food court. It represents the final step of the sensemaking process since P_I is the measure of performance for the system in this case study. During a control interval, the instantaneous quanta concentration at each susceptible diner's location $n_{q(t,x,y,z)}$ (quanta/m^3) can be evaluated using the following equation which includes the molar concentrations of infectious aerosols exported from the previous module as one of the terms:

$$n_{q(t,x,y,z)} = \frac{n_{m(t,x,y,z)} \cdot M_w}{\rho_w} \cdot c_v \cdot c_i \cdot e^{-IVRR(t-t_{start})} \quad (18)$$

where $n_{m(t,x,y,z)}$ (kmol/m^3) is the average molar concentration of exhaled water vapor in the breathing zone of the susceptible diner with coordinates (x, y, z) at time t (h), M_w (kg/kmol) is the molecular weight of water, c_v (RNA copies/mL) is the viral load in the sputum, c_i (quanta/RNA copies) is the conversion factor defined as the ratio between one infectious quantum and the infectious dose expressed in viral RNA copies, $IVRR$ (h^{-1}) is the infectious virus removal rate, and t_{start} is the starting time of the control interval (h). It should be noted that $n_{m(t,x,y,z)}$ is calculated from the exported data of the CFD simulation in module two. The SARS-CoV-2 viral load in the sputum is assumed to be 10^7 RNA copies/mL which represents an average value within the range of 10^3–10^{11} copies/mL reported in the literature (Pan et al., 2020; Woelfel et al., 2020; Zou et al., 2020). The conversion factor, c_i, can be expressed as the reciprocal of the product of the number of viral RNA copies needed to form a plaque-forming unit (PFU), c_{RNA} , and the quanta-to-PFU conversion factor, c_{PFU}. The values of c_{RNA} and c_{PFU} are taken to be 1.3× 10^2 RNA copies/PFU (Fears et al., 2020) and 2.1 × 10^2 PFU/quanta (Watanabe et al., 2010), respectively. The removal

rate of SARS-CoV-2 is the sum of the deposition rate of super-micrometric particles and the viral inactivation rate which are taken to be 0.24 h^{-1} (Chatoutsidou and Lazaridis, 2019) and 0.63 h^{-1} (van Doremalen et al., 2020), respectively. The dose of quanta received by each susceptible diner during the control interval D_q (quanta) can then be evaluated as:

$$D_q = IR \int_{t_{start}}^{t_{start}+t_i} n_{q(t,x,y,z)} dt \quad (19)$$

Subsequently, the P_I of each diner can be evaluated using the exponential dose-response model below that is widely used in the literature to simplify the random distribution of aerosolized pathogens in the air as an exponential equation (Sze To and Chao, 2010; Watanabe et al., 2010):

$$P_I = 1 - e^{-D_q} \quad (20)$$

3.3.4. Rule-based ventilation controller

Representing the recalibration step of the dynamic response strategy, the final module of the digital-twin control compares the maximum P_I observed during a control interval against P_{ST} (refer to Section 3.1) to decide on the adaptative change in V_h for the next control interval (Figure 6). Diners whose P_I exceed P_{ST} during a control interval are termed as at-risk diners in this study. If P_{ST} is exceeded and V_h is below the minimum rate recommended by the WHO (World Health Organization, 2021) for reducing the risk of COVID-19 transmission in non-residential settings, i.e., 10 L/s/person, V_h for the next control interval is set to be the recommended rate. Otherwise, it is set to the current rate increased by a correction factor K. If all P_I are below P_{ST}, it is set to the current rate decreased by K. V_h is not allowed to decrease below the minimum value recommended by ASHRAE 62.1-2022 (American Society of Heating, Refrigerating and Air-Conditioning Engineers, 2022) for the indoor space of interest. For the food court case study, this minimum V_h is 1513 m^3/h, i.e., 3.8 L/s/person assuming maximum occupancy of 40 diners. The actualization

of the updated V_h marks the end of one iteration of the digital-twin control loop. This updated V_h is then utilized as one of the inputs for the CFD simulation in the next iteration.

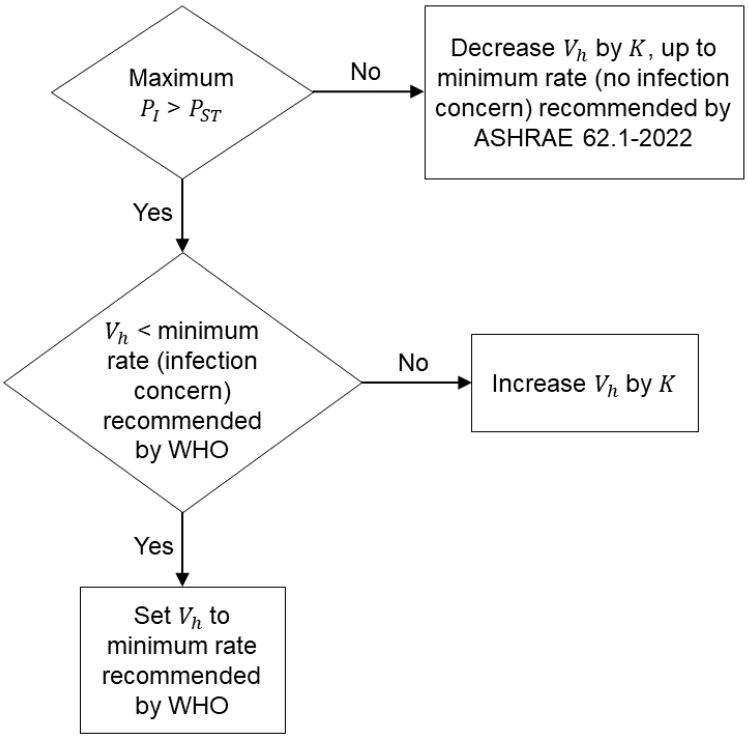

Fig 6. Decision flowchart of the infection-risk-centric rule-based ventilation controller

3.4. Energy use of ventilation system required for resilience

To understand the tradeoff between resilience and energy use, the energy used by the ventilation system during a control interval E (kWh) can be evaluated as:

$$E = (P_{AC} + P_{MV})(t_{end} - t_{start}) \tag{21}$$

where P_{AC} (kW) is the air-conditioning power consumption, P_{MV} (kW) is the mechanical ventilation power consumption, and t_{end} is the ending time of the control interval (h). P_{AC} and P_{MV} can be estimated by the equations as follows (Wang et al., 2021):

$$P_{AC} = Q/COP \tag{22}$$

$$Q = V_h \rho_{air} C_p (T_{out} - T_{in})/3600 \tag{23}$$

$$P_{MV} = \beta V_s^3 \quad (24)$$

where Q (kW) is the ventilation load, COP is the coefficient of performance of the air-conditioning subsystem, ρ_{air} (kg/m^3) is the density of air, C_p (kJ/(kg°C)) is the specific heat capacity of air at constant pressure, T_{in} and T_{out} (°C) are the indoor and outdoor temperatures, respectively, β (kWm^{-9}s^3) is the coefficient obtained from the catalog of the fan, and V_s is the ventilation rate (m^3/s). COP and β are set as 4.2 and 0.8 kWm^{-9}s^3, respectively (Wang et al., 2021).

3.5. Ventilation scenarios for assessment of real-time resilience

To assess the added value of real-time resilience enabled by the digital-twin control of the ventilation system, the percentage improvements in the metrics T_d, $r(t_{df})$, $\Psi_{loss}(t_{df})$, $\overline{\nabla P_D}(t_{df})$ and $\overline{\nabla P_R}(t_{df})$ (Section 2), which were derived from the trajectories of the P_I of the diners, and the energy use of the ventilation system were compared across six ventilation scenarios in the same food court setting. C1 is the baseline scenario where the ventilation system operates at a fixed rate of 10L/s/person corresponding to the WHO recommended minimum rate for COVID-19 control purposes. This represents a static mitigation response to the disruption event of an infectious diner being present in the food court. T1, T2, T3, T4, and T5 are the real-time resilience scenarios where the ventilation system operates dynamically under the digital-twin control with the parameter K of the rule-based ventilation controller set at 10%, 20%, 30%, 40%, and 50%, respectively. A range of K was studied to reflect varying adaptive capacities of the system. In each scenario, the P_I of the diners were tracked for a duration of one hour and the duration of a control interval was set as five minutes. To ensure fair comparisons across the scenarios, a few simplifying assumptions were taken. The locations of the diners are restricted to the 40 seats in the food court which are assumed to be always occupied during the monitoring duration. The diner at seat 23, which is in the middle

of the food court, is designated as the sole infectious individual while the other diners are susceptible individuals. To study the recovery phase of the disruption, the infectious diner is simulated to be present only in the first 30 minutes.

The aerosol dispersion simulator in the digital-twin control is assumed to work in real time. Although physics-based models such as the CFD simulations used in the control are typically too time consuming for real-time applications, numerous studies have demonstrated that machine-learning-based models can be used as a surrogate to obtain the desired predictions (Jurado et al., 2022; Mirzaei et al., 2022; Seo et al., 2022). Since the purpose of the case study is to serve as an illustrative example of how real-time resilience can be enabled and assessed in a realistic setting, the development of such surrogate models, though important, is out of the scope of the study. Additionally, the occupancy detector in the control is assumed to be incapable of identifying and tracking individual diners over time which would require facial recognition or wearable technologies that are not typically implemented in a food court setting. Consequently, the accumulation of the dose of infectious aerosols inhaled by a diner across control intervals are not considered. Exposures during each of the control interval were used as a proxy for real-time infection risk of the diners instead.

4. Results

The resilience of the diners against the transmission of COVID-19 in the studied case is an outcome of the interaction between the ventilation scenario and the locations of the susceptible and infectious diners. In the baseline scenario C1, 15 of the 40 diners were at risk, that is, their P_I exceeded P_{ST} within the monitored duration. The analysis of resilience was conducted only for these at-risk diners whose P_I were unacceptable for one or more control intervals. Given that the

at-risk diners were located only at tables immediately adjacent to the table containing the infectious diner, it can be inferred that the concentrations of infectious aerosols decreased to negligible levels beyond approximately 10 m from the source in the simulated conditions.

Considering the overall resilience of the diners as the sum of the individual resilience of each diner, the digital-twin-controlled ventilation in T1 to T5 with K ranging from 10% to 50% improved the overall T_d (26%–61%), $\Psi_{loss}(t_{df})$ (2%–39%), and $\overline{\nabla P_R}(t_{df})$ (26%–74%) relative to C1 (Table 2). As K increases, the percentage improvement of individual T_d and $\Psi_{loss}(t_{df})$ increased monotonically for all the diners with the only exception being the decrease from T4 to T5 for the diner at seat 20 (Table 3). K of 20% or more is required to ensure all at-risk diners have improved individual T_d compared to C1 while K of 30% or more is required to ensure the same for individual $\Psi_{loss}(t_{df})$. In contrast, there were no significant improvements to the overall $r(t_{df})$ (< 3%) and significantly worse overall $\overline{\nabla P_D}(t_{df})$ were observed in T1 and T5. The individual resilience metrics of $r(t_{df})$, $\overline{\nabla P_D}(t_{df})$ and $\overline{\nabla P_R}(t_{df})$ showed mixed trends when K increases. Even with K at 50%, these metrics did not improve for every at-risk diner and the digital-twin-controlled ventilation cannot prevent P_I from exceeding P_{ST} for all the diners.

While both the digital-twin-controlled ventilation scheme and higher K of the controller are hypothesized to improve the resilience of all the diners by introducing a greater quantity of clean outdoor air when P_I are estimated to be unacceptable, their effects on the individual resilience of the diners vary significantly based on the locations of the diners. This spatial variation in the effects of ventilation is so high that the individual resilience metrics at some seats declined in T1 to T5 instead of increasing as hypothesized (red values in Table 3). For the purposes of discussing the results of the case study, seats 25 to 40 are considered ‘upwind’ of the infectious diner, seats 17 to 24 are considered ‘adjacent’ while seats 1 to 16 are considered ‘downwind’.

Generally, the at-risk diners that were located upwind or in a different row of tables from the infectious diner, i.e., at seats 18, 26, 29, and 30, had higher percentage improvements in individual T_d, $r(t_{df})$, and $\Psi_{loss}(t_{df})$ (Table 3). Moreover, they consistently exhibited increasing improvements in these individual resilience metrics when higher levels of K were implemented. Except for the diner at seat 28, all of them achieved improvements of sufficient magnitude under digital-twin-controlled ventilation at a certain level of K such that their P_I were maintained at acceptable levels throughout the monitored duration and they became no longer at risk in those ventilation scenarios. Expectedly, the diner at seat 24, who is the closest to the infectious diner, had the lowest resilience, accounting for up to 28%, 87%, and 91% of the overall T_d, $r(t_{df})$, and $\Psi_{loss}(t_{df})$ of the diners, respectively (Appendix A). With increasing levels of K, the percentage improvement in $\Psi_{loss}(t_{df})$ for the diner at seat 24 increased to 36% but the improvements in T_d and $r(t_{df})$ did not increase significantly, with maximum magnitudes at <2% and <6%, respectively. The higher energy use associated with higher levels of K are shown in Table 4. Figure 7 visualizes the spatial distribution of the concentration of infectious aerosols and the streamlines induced by the supply air vents upwind of the infectious diner, which influence the individual resilience of the diners, at the snapshot of 30 minutes.

Table 2. Percentage improvement in the overall resilience of the at-risk diners as measured by T_d, $r(t_{df})$, $\Psi_{loss}(t_{df})$, $\overline{\nabla P_D}(t_{df})$ and $\overline{\nabla P_R}(t_{df})$ considering the entire tracked duration of one hour and all the diners. Cells shaded in green and red represent improved and worse resilience metric values compared to C1, respectively.

Ventilation scenario	Percentage improvement in overall resilience for at-risk diners (%)				
	T_d	$r(t_{df})$	$\Psi_{loss}(t_{df})$	$\overline{\nabla P_D}(t_{df})$	$\overline{\nabla P_R}(t_{df})$
T1	26	-2	2	-26	26
T2	43	-2	14	5	66
T3	50	1	28	6	74
T4	57	3	36	7	59
T5	61	3	39	-59	67

Table 3. Percentage improvement in the individual resilience of the at-risk diners as measured by the metrics T_d, $r(t_{df})$, $\Psi_{loss}(t_{df})$, $\overline{\nabla P_D}(t_{df})$ and $\overline{\nabla P_R}(t_{df})$ considering the entire tracked duration of one hour. Cells shaded in green and red represent improved and worse resilience metric values compared to C1, respectively, while cells shaded in darker green represent improvements of sufficient magnitude such that the diners are no longer at risk, i.e., their P_I were maintained at acceptable levels throughout the monitored duration. Individual diners are identified by their seat numbers which are grouped according to the positions relative to the infectious diner.

		Percentage improvement in individual resilience metric (%)														
		T_d					$r(t_{df})$					$\Psi_{loss}(t_{df})$				
	Seat	T1	T2	T3	T4	T5	T1	T2	T3	T4	T5	T1	T2	T3	T4	T5
downwind	11	27	50	60	67	70	-54	-177	-201	-70	-119	-26	-24	12	38	48
	12	25	48	58	66	68	-18	-15	-6	21	4	8	38	57	67	71
	15	-6	10	20	35	48	-32	-32	15	20	15	-25	-2	24	40	51
	16	22	36	46	53	60	12	9	14	20	27	27	46	64	72	76
adjacent	18	100	100	100	100	100	100	100	100	100	100	100	100	100	100	100
	19	1	3	6	11	12	-7	1	-5	1	0	-1	14	21	35	39
	20	7	11	11	12	11	-6	-2	-5	4	-2	1	5	9	17	14
	24	0	0	1	5	6	-1	-2	2	1	2	1	12	25	33	36
upwind	26	100	100	100	100	100	100	100	100	100	100	100	100	100	100	100
	27	47	68	76	85	100	30	70	64	78	100	58	89	92	97	100
	28	43	55	63	73	79	-71	7	14	19	47	-17	52	65	78	89
	29	35	100	100	100	100	20	100	100	100	100	48	100	100	100	100
	30	84	100	100	100	100	83	100	100	100	100	97	100	100	100	100
	31	43	93	100	100	100	45	92	100	100	100	48	99	100	100	100
	32	31	61	74	92	100	-55	60	66	88	100	-7	84	92	99	100

		$\overline{\nabla P_D}(t_{df})$					$\overline{\nabla P_R}(t_{df})$				
	Seat	T1	T2	T3	T4	T5	T1	T2	T3	T4	T5
downwind	11	-35	-161	-316	-175	-549	180	576	652	769	496
	12	-50	-119	-101	-222	-266	34	75	144	73	126
	15	-83	-89	-48	-196	-205	-34	-3	-11	-17	12
	16	-28	-31	-26	-20	-13	-2	28	54	64	106
adjacent	18	-	-	-	-	-	-	-	-	-	-
	19	8	23	43	59	75	5	-2	-4	-13	-17
	20	-7	-4	9	19	30	6	30	30	19	19
	24	-7	37	44	47	21	7	19	6	1	-20
upwind	26	-	-	-	-	-	-	-	-	-	-
	27	58	64	53	-8	-	41	33	171	-23	-
	28	-286	-33	-24	-189	-56	98	180	337	144	198
	29	-61	-	-	-	-	-10	-	-	-	-
	30	4	-	-	-	-	10	-	-	-	-
	31	20	43	-	-	-	204	161	-	-	-
	32	-142	-58	-12	-149	-	32	-8	75	-30	-

Table 4. Energy use by the ventilation system in the different ventilation scenarios

	C1	T1	T2	T3	T4	T5
Energy use (kWh)	1.6	3.6	5.9	15.5	48.6	162.7

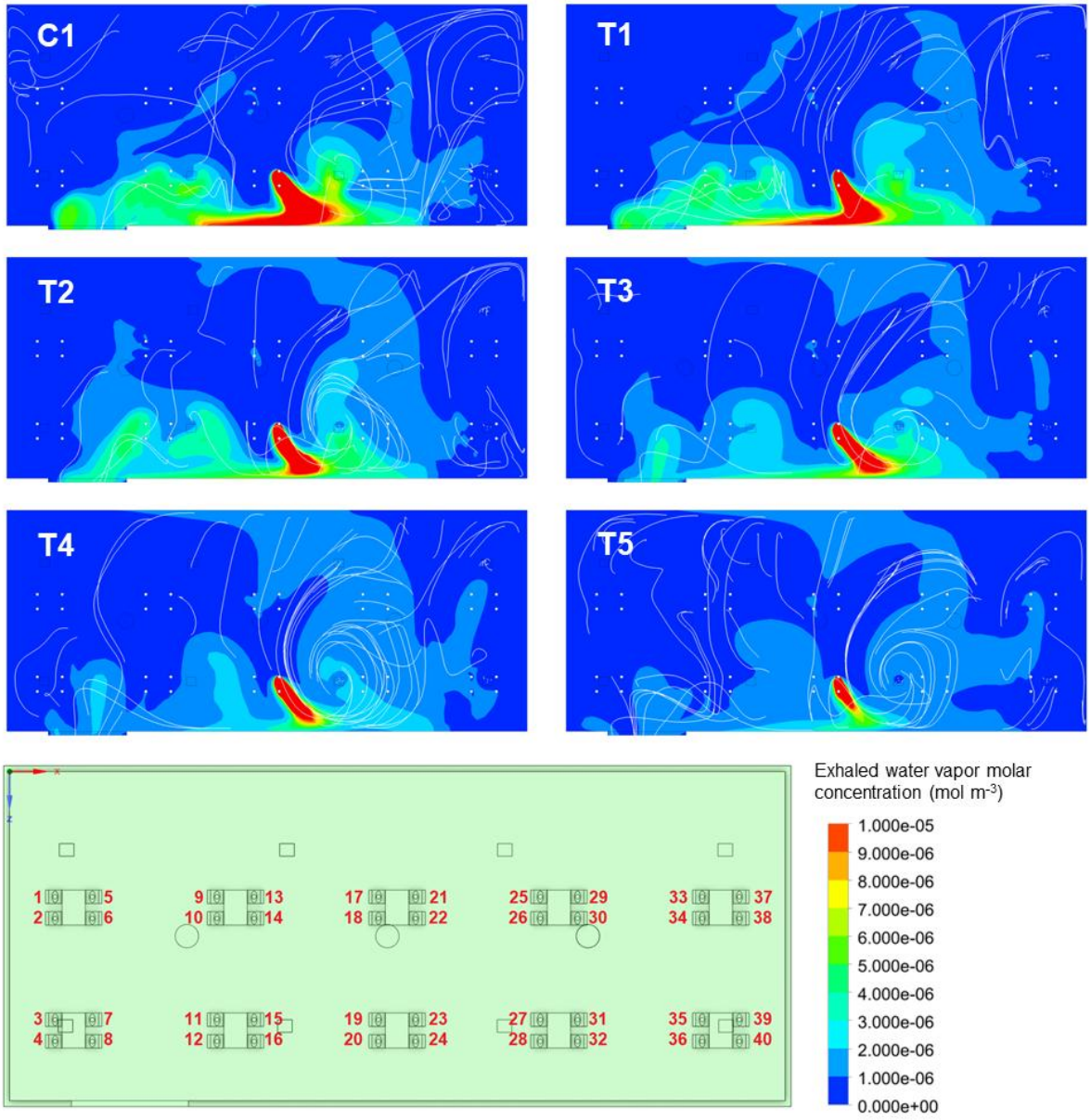

Fig 7. Contours of the molar concentrations of exhaled water vapor which were used as a proxy for the emitted virus-laden aerosols with an overlay of the streamlines induced by the supply air vents upwind of the infectious diner at seat 24, for the baseline ventilation scenario (C1) and the scenarios with digital-twin-controlled ventilation (T1–T5).

5. Discussion

5.1 Digital-twin-controlled ventilation for real-time resilience against the transmission of airborne infectious diseases

Generally, the case study demonstrated how the added value of real-time resilience can be quantified and how such resilience can be enabled by a dynamic response strategy that involves 1) monitoring, where the digital twin of the given indoor space and ventilation system observes occupancy and ventilation in real time, 2) sensemaking, where the twin uses the real-time information streams to conduct tempo-spatial assessment of P_I, and 3) recalibration of the ventilation responses to enhance the resilience of the diners against airborne infection. In the studied case, since the response to the disruption involves the adjustment of the ventilation rate V_h, i.e., the volume flow rate of pathogen-free air supplied to the space, the adaptive capacity of the system is defined by the correction factor K which quantifies the magnitude of the V_h adjustments between consecutive control intervals. The response of introducing clean air to a space serves to reduce P_I by diluting the concentrations of infectious airborne aerosols in the space and removing them from the space through air volume changes (Arpino et al., 2022; Morawska et al., 2021; Sha et al., 2021). These dilution and removal effects are reflected in the improvements to the overall T_d, $\Psi_{loss}(t_{df})$, and $\overline{\nabla P_R}(t_{df})$ relative to C1 when the digital-twin-controlled ventilation was implemented.

With respect to the individual resilience of the diners, the simulation results revealed two limitations of the investigated response. Firstly, the effect of V_h on P_I and, correspondingly, the individual resilience of the diner is limited in magnitude. The results showed that using adaptive mixing ventilation as the sole mitigation response was insufficient to maintain the P_I of all diners at acceptable levels in the presence of an infected diner with a dwell duration of 30 minutes. In fact, the adaptive ventilation implemented in T1 to T5 prevented the exceedance of P_{ST} only for

the at-risk diners with lower T_d and $\Psi_{loss}(t_{df})$ (i.e., higher resilience) in C1, namely, those who are upwind of or in a different row of tables from the infectious diner. Increasing K beyond 50% is unlikely to be a feasible way to prevent the exceedance of P_{ST} for susceptible diners who are sitting immediately adjacent an infectious diner while ensuring the indoor air velocities are not high enough to result in uncomfortable drafts. Secondly, the effect of V_h on the individual resilience of each diner is neither linear nor always positive, with the direction and strength of the relationship dependent on the location of the diner. While increasing V_h of a mixing ventilation system like in T1 to T5 can increase the resilience of some diners, it may also reduce the resilience of other diners. For instance, in terms of $\Psi_{loss}(t_{df})$, the diners at seats 11, 15, 19, 28, and 32 had worse (i.e., higher) values in T1 or T2 than in C1. The observation that increasing V_h does not necessarily decrease the P_I for all occupants of a space is corroborated by previous experiments and simulations (Berlanga et al., 2018; Pantelic and Tham, 2013; Wang et al., 2018). A possible explanation is that the turbulent air flows generated from the higher V_h could increase the rate of the lateral dispersion of the infectious aerosols and recirculate the aerosols within some locations (Vuorinen et al., 2020). This leads to higher $r(t_{df})$ and $\overline{\nabla P_D}(t_{df})$ and lower $\overline{\nabla P_R}(t_{df})$ relative to C1 for the diners whose breathing zones intersect the flow paths of the aerosols. Specific to the case study, the decline in these individual resilience metrics could be attributed to the air flows from the location of the infectious diner that were predominantly 1) towards the nearest wall across the susceptible diner at seat 24, 2) towards the entrance/exit of the food court, passing by the table downwind with seats 11, 12, 15 and 16, and 3) recirculating within an area upwind covering seats 25–32 (Figure 7). However, the results also indicate that there is an optimal value for K beyond which the avoidance of Ψ_{loss} and T_d are positive for all at-risk diners. This implies that when K is sufficiently high, the positive effects of dilution and removal associated with higher V_h outweighs

the negative effects of lateral dispersion and potential recirculation due to the turbulent air flows. Additionally, the combined effects of increased dispersion and removal of aerosols at higher levels of K might account for the spikier resilience curves observed in those ventilation scenarios for the diners at seats 11, 12, 20, and 28, which are characterized by higher $r(t_{df})$ and $\overline{\nabla P_D}(t_{df})$ but higher $\overline{\nabla P_R}(t_{df})$ and lower T_d and $\Psi_{loss}(t_{df})$.

Given the potential undesirable outcomes of increasing V_h in a mixing ventilation system, a possible alternative is to use displacement ventilation which transports the aerosols vertically towards the ceiling and away from the breathing zones of all diners (Seo et al., 2022; Villafruela et al., 2019). With displacement ventilation, the lateral dispersion and homogenization of the aerosols within the occupied zone are expected to be reduced, resulting in more pathogen-free regions (Bhagat and Linden, 2020). Nonetheless, the lock-up height of the infectious aerosols that is induced by the vertical displacement should be checked to lie above the breathing zones of the diners (Liu et al., 2020; Mui et al., 2009). Like mixing ventilation, the V_h and the number and position of air inlets and outlets could be investigated to improve the resilience enhancement capability of the displacement ventilation system (Qian et al., 2006). Another option is personal ventilation which can remove the aerosols close to the source and target the greatly heightened P_I of occupants in close contact with infectors, e.g., at seat 24 which the mixing ventilation system is unable to target specifically (Izadyar and Miller, 2022; Pantelic and Tham, 2013).

In addition to determining the appropriate ventilation response, the tempo-spatial assessment of P_I in the sensemaking step that is conducted by the digital twin can be used to identify transient safe zones as they evolve over the disruption event. This is especially important for larger spaces with less well-mixed air and could inform evacuation routes in the context of emergencies involving acutely hazardous air contaminants. The importance of considering the

tempo-spatial variations for P_I in indoor settings is documented in studies of airborne infection risks in vehicle cabins (Pirouz et al., 2021; Arpino et al., 2022; Wang et al., 2022), offices (Motamedi et al., 2022), and grocery stores (Zhang et al., 2022).

5.2 Trade-off between resilience and energy

The trade-off between enhancement of resilience against transmission of airborne infectious diseases via mechanical ventilation and energy use of the ventilation system is evident from the simulation results. Consequently, an evaluation of the health costs of infection and energy costs of the physical systems may be necessary before mechanical ventilation solutions for infection risk mitigation are more widely adopted. Comparing C1 and T4 as an example, the knowledge of the different costs involved could help building managers decide whether the additional 47 kWh of energy use in T4 is worthwhile for the 57% and 36% improvements in overall T_d and $\Psi_{loss}(t_{df})$, respectively. In addition to mechanical ventilation, which can be energy intensive, air filtration and UV disinfection are alternative engineering solutions for enhancing resilience against airborne infection. Zhu et al. (2012) studied airborne influenza infection in public transport using CFD simulations and reported that the infection risk when air is recirculated but filtered with a HEPA filter is approximately equal to the infection risk when the air is not recirculated and there is no filtration. This suggests that air filters could be as effective as mechanical ventilation in mitigating infection risks. Buchan et al. (2020) reported that low dose far-UVC lighting could increase the removal of airborne SARS-Cov-2 aerosols by 50–85% compared to ventilation alone and should be considered when increasing V_h to the target level is not feasible. Future studies could compare the energy-efficiency and the effectiveness of these

engineering solutions in resilience enhancement and investigate their potential synergies in different scenarios.

5.3 General lessons for real-time resilience

To enable real-time resilience in a physical system, a model of the system that is both dynamic and retains memory of historical performances needs to be developed. The continuously updated aerosol dispersion simulator in the case study is one such example and it is crucial for making assessments and predictions of system performance which, in turn, inform decision making for resilience objectives (Campos et al., 2022). Additionally, to design effective system control for real-time resilience, it should be clear how the selected control parameters that determine system responses affect the measure(s) of the performance of interest. As in the studied case, the relationship between the control parameter and resilience is typically complex and should be investigated across the full range of possible scenarios to build a comprehensive control design.

6. Conclusion

This study develops an assessment method for real-time resilience and proposes the percentage improvements in T_d, $r(t)$, $\Psi_{loss}(t)$, $\overline{\nabla P_D}(t)$ and $\overline{\nabla P_R}(t)$ as metrics to quantify the added value of having the capacity to continuously recalibrate responses to an ongoing disruption. The application of these metrics for evaluating the effectiveness of a dynamic response strategy for disruption mitigation was demonstrated using a novel case study of airborne infection transmission in an indoor food court with a digital-twin-controlled ventilation system. The comparative simulations from the case study showed that:

1) A digital twin of a given indoor space with a conventional mixing ventilation system can enhance the overall resilience of the occupants against the transmission of airborne infectious diseases by enabling a dynamic response strategy that comprises of continuous monitoring of occupancy and ventilation, sensemaking in terms of tempo-spatial assessment of P_I, and recalibration of V_h as a mitigation action. The enhancements in overall resilience were quantified by the improvements in the overall T_d (26%–61%), $\Psi_{loss}(t_{df})$ (2%–39%), and $\overline{\nabla P_R}(t_{df})$ (26%–74%).
2) The effect of V_h on the individual resilience of the occupants is highly spatial and could be limited in magnitude depending on the locations of the susceptible and infectious occupants. While the spatial patterns for the resilience metrics are site-specific, the general insight that increasing V_h of a mixing ventilation system could lead to increased dilution and removal but also greater lateral dispersion and potential recirculation, which have opposing effects on the resilience, was inferred from the simulation results.
3) The tradeoff between the enhancement of resilience via mechanical ventilation and the energy use of the ventilation system limits the applicability of adjustments of V_h as a response and highlights the need to establish the health costs of infection and the energy costs of the physical systems in the same units so that they can be weighed against each other for decision making.

Future work in real-time resilience should investigate how the evaluation metrics proposed in this study could be used in tandem with traditional performance objectives to enable systems with autonomy and decision makers to make optimal decisions during a disruption event. Moreover, the further development of intelligent models that could conduct monitoring and sensemaking, as

well as recalibrate responses in a continuous and timely manner is essential to enable real-time resilience for physical systems in the future.

Acknowledgement

This work is an outcome of the Future Resilient Systems project "Digital Twin Enabled System Resilience" at the Singapore-ETH Centre (SEC) supported by the National Research Foundation, Prime Minister's Office, Singapore under its Campus for Research Excellence and Technological Enterprise (CREATE) programme.

Conflict of interest

The authors declare that they have no known competing financial interests or personal relationships that could have appeared to influence the work reported in this paper.

Data availability statement

The data that support the findings of this study are available from the corresponding author upon reasonable request.

References

Adams, W.C., 1993. Measurement of breathing rate and volume in routinely performed daily activities. Final Report Contract.

American Society of Heating, Refrigerating and Air-Conditioning Engineers, 2022. ASHRAE Standard 62.1-2022, Ventilation for acceptable indoor air quality.

ANSYS, Inc., 2021. Ansys Fluent Theory Guide.

Arpino, F., Grossi, G., Cortellessa, G., Mikszewski, A., Morawska, L., Buonanno, G., Stabile, L., 2022. Risk of SARS-CoV-2 in a car cabin assessed through 3D CFD simulations. Indoor Air 32, e13012. https://doi.org/10.1111/ina.13012

Bécue, A., Maia, E., Feeken, L., Borchers, P., Praça, I., 2020. A New Concept of Digital Twin Supporting Optimization and Resilience of Factories of the Future. Applied Sciences 10, 4482. https://doi.org/10.3390/app10134482

Berlanga, F.A., de Adana, M.R., Olmedo, I., Villafruela, J.M., San José, J.F., Castro, F., 2018. Experimental evaluation of thermal comfort, ventilation performance indices and exposure to airborne contaminant in an airborne infection isolation room equipped with a displacement air distribution system. Energy and Buildings 158, 209–221. https://doi.org/10.1016/j.enbuild.2017.09.100

Bhagat, R.K., Linden, P.F., 2020. Displacement ventilation: a viable ventilation strategy for makeshift hospitals and public buildings to contain COVID-19 and other airborne diseases. Royal Society open science 7, 200680.

Boyd, E., Cornforth, R.J., Lamb, P.J., Tarhule, A., Lélé, M.I., Brouder, A., 2013. Building resilience to face recurring environmental crisis in African Sahel. Nature Clim Change 3, 631–637. https://doi.org/10.1038/nclimate1856

Brucherseifer, E., Winter, H., Mentges, A., Mühlhäuser, M., Hellmann, M., 2021. Digital Twin conceptual framework for improving critical infrastructure resilience. at - Automatisierungstechnik 69, 1062–1080. https://doi.org/10.1515/auto-2021-0104

Buchan, A.G., Yang, L., Atkinson, K.D., 2020. Predicting airborne coronavirus inactivation by far-UVC in populated rooms using a high-fidelity coupled radiation-CFD model. Sci Rep 10, 19659. https://doi.org/10.1038/s41598-020-76597-y

Buonanno, G., Morawska, L., Stabile, L., 2020. Quantitative assessment of the risk of airborne transmission of SARS-CoV-2 infection: Prospective and retrospective applications. Environment International 145, 106112. https://doi.org/10.1016/j.envint.2020.106112

Burgos, D., Ivanov, D., 2021. Food retail supply chain resilience and the COVID-19 pandemic: A digital twin-based impact analysis and improvement directions. Transportation Research Part E: Logistics and Transportation Review 152, 102412. https://doi.org/10.1016/j.tre.2021.102412

Campos, A.T., dos Santos, C.H., Gabriel, G.T., Montevechi, J.A.B., 2022. Safety assessment for temporary hospitals during the COVID-19 pandemic: A simulation approach. Safety Science 147, 105642. https://doi.org/10.1016/j.ssci.2021.105642

Chatoutsidou, S.E., Lazaridis, M., 2019. Assessment of the impact of particulate dry deposition on soiling of indoor cultural heritage objects found in churches and museums/libraries. Journal of Cultural Heritage 39, 221–228. https://doi.org/10.1016/j.culher.2019.02.017

Chitaru, G., Berville, C., Dogeanu, A., 2018. Numerical simulation and comparison of two ventilation methods for a restaurant–displacement vs mixed flow ventilation, in: E3S Web of Conferences. EDP Sciences, p. 01012.

Eirinakis, P., Lounis, S., Plitsos, S., Arampatzis, G., Kalaboukas, K., Kenda, K., Lu, J., Rožanec, J.M., Stojanovic, N., 2022. Cognitive Digital Twins for Resilience in Production: A Conceptual Framework. Information 13, 33. https://doi.org/10.3390/info13010033

Fears, A.C., Klimstra, W.B., Duprex, P., Hartman, A., Weaver, S.C., Plante, K.C., Mirchandani, D., Plante, J.A., Aguilar, P.V., Fernández, D., Nalca, A., Totura, A., Dyer, D., Kearney, B., Lackemeyer, M., Bohannon, J.K., Johnson, R., Garry, R.F., Reed, D.S., Roy, C.J., 2020. Comparative dynamic aerosol efficiencies of three emergent coronaviruses and the unusual persistence of SARS-CoV-2 in aerosol suspensions. medRxiv 2020.04.13.20063784. https://doi.org/10.1101/2020.04.13.20063784

Flammini, F., 2021. Digital twins as run-time predictive models for the resilience of cyber-physical systems: a conceptual framework. Phil. Trans. R. Soc. A. 379, 20200369. https://doi.org/10.1098/rsta.2020.0369

Ho, C.K., 2021. Modeling airborne pathogen transport and transmission risks of SARS-CoV-2. Applied Mathematical Modelling 95, 297–319. https://doi.org/10.1016/j.apm.2021.02.018

Ho, C.K., Binns, R., 2021. Modeling and mitigating airborne pathogen risk factors in school buses. International Communications in Heat and Mass Transfer 129, 105663. https://doi.org/10.1016/j.icheatmasstransfer.2021.105663

Hollnagel, E., Woods, D.D., Leveson, N., 2006. Resilience engineering: Concepts and precepts. Ashgate Publishing, Ltd.

Izadyar, N., Miller, W., 2022. Ventilation strategies and design impacts on indoor airborne transmission: A review. Building and Environment 218, 109158. https://doi.org/10.1016/j.buildenv.2022.109158

Jurado, X., Reiminger, N., Benmoussa, M., Vazquez, J., Wemmert, C., 2022. Deep learning methods evaluation to predict air quality based on Computational Fluid Dynamics. Expert Systems with Applications 203, 117294. https://doi.org/10.1016/j.eswa.2022.117294

Kim, S., Eun, Y., Park, K.-J., 2021. Stealthy Sensor Attack Detection and Real-Time Performance Recovery for Resilient CPS. IEEE Trans. Ind. Inf. 17, 7412–7422. https://doi.org/10.1109/TII.2021.3052182

Lei, S., Wang, J., Chen, C., Hou, Y., 2016. Mobile Emergency Generator Pre-Positioning and Real-Time Allocation for Resilient Response to Natural Disasters. IEEE Trans. Smart Grid 1–1. https://doi.org/10.1109/TSG.2016.2605692

Liu, F., Qian, H., Luo, Z., Wang, S., Zheng, X., 2020. A laboratory study of the expiratory airflow and particle dispersion in the stratified indoor environment. Building and Environment 180, 106988. https://doi.org/10.1016/j.buildenv.2020.106988

Mirzaei, P.A., Moshfeghi, M., Motamedi, H., Sheikhnejad, Y., Bordbar, H., 2022. A simplified tempo-spatial model to predict airborne pathogen release risk in enclosed spaces: An Eulerian-Lagrangian CFD approach. Building and Environment 207, 108428. https://doi.org/10.1016/j.buildenv.2021.108428

Morawska, L., Allen, J., Bahnfleth, W., Bluyssen, P.M., Boerstra, A., Buonanno, G., Cao, J., Dancer, S.J., Floto, A., Franchimon, F., Greenhalgh, T., Haworth, C., Hogeling, J., Isaxon, C., Jimenez, J.L., Kurnitski, J., Li, Y., Loomans, M., Marks, G., Marr, L.C., Mazzarella, L., Melikov, A.K., Miller, S., Milton, D.K., Nazaroff, W., Nielsen, P.V., Noakes, C., Peccia, J., Prather, K., Querol, X., Sekhar, C., Seppänen, O., Tanabe, S., Tang, J.W., Tellier, R., Tham, K.W., Wargocki, P., Wierzbicka, A., Yao, M., 2021. A paradigm shift to combat indoor respiratory infection. Science 372, 689–691. https://doi.org/10.1126/science.abg2025

Motamedi, H., Shirzadi, M., Tominaga, Y., Mirzaei, P.A., 2022. CFD modeling of airborne pathogen transmission of COVID-19 in confined spaces under different ventilation strategies. Sustainable Cities and Society 76, 103397. https://doi.org/10.1016/j.scs.2021.103397

Mui, K.W., Wong, L.T., Wu, C.L., Lai, A.C.K., 2009. Numerical modeling of exhaled droplet nuclei dispersion and mixing in indoor environments. Journal of Hazardous Materials 167, 736–744. https://doi.org/10.1016/j.jhazmat.2009.01.041

Noebels, M., Preece, R., Panteli, M., 2022. A machine learning approach for real-time selection of preventive actions improving power network resilience. IET Generation, Transmission & Distribution 16, 181–192.
Pan, Y., Zhang, D., Yang, P., Poon, L.L.M., Wang, Q., 2020. Viral load of SARS-CoV-2 in clinical samples. The Lancet Infectious Diseases 20, 411–412. https://doi.org/10.1016/S1473-3099(20)30113-4
Pantelic, J., Tham, K.W., 2013. Adequacy of air change rate as the sole indicator of an air distribution system's effectiveness to mitigate airborne infectious disease transmission caused by a cough release in the room with overhead mixing ventilation: A case study. HVAC&R Research 19, 947–961. https://doi.org/10.1080/10789669.2013.842447
Pirouz, B., Mazzeo, D., Palermo, S.A., Naghib, S.N., Turco, M., Piro, P., 2021. CFD Investigation of Vehicle's Ventilation Systems and Analysis of ACH in Typical Airplanes, Cars, and Buses. Sustainability 13, 6799. https://doi.org/10.3390/su13126799
Qian, H., Li, Y., Nielsen, P.V., Hyldgaard, C.E., Wong, T.W., Chwang, A.T.Y., 2006. Dispersion of exhaled droplet nuclei in a two-bed hospital ward with three different ventilation systems. Indoor Air 16, 111–128. https://doi.org/10.1111/j.1600-0668.2005.00407.x
Rasheed, A., San, O., Kvamsdal, T., 2019. Digital Twin: Values, Challenges and Enablers.
Saad, A., Faddel, S., Youssef, T., Mohammed, O.A., 2020. On the Implementation of IoT-Based Digital Twin for Networked Microgrids Resiliency Against Cyber Attacks. IEEE Trans. Smart Grid 11, 5138–5150. https://doi.org/10.1109/TSG.2020.3000958
Seo, S.-K., Yoon, Y.-G., Lee, J., Na, J., Lee, C.-J., 2022. Deep Neural Network-based Optimization Framework for Safety Evacuation Route during Toxic Gas Leak Incidents. Reliability Engineering & System Safety 218, 108102. https://doi.org/10.1016/j.ress.2021.108102
Sha, H., Zhang, X., Qi, D., 2021. Optimal control of high-rise building mechanical ventilation system for achieving low risk of COVID-19 transmission and ventilative cooling. Sustain Cities Soc 74, 103256. https://doi.org/10.1016/j.scs.2021.103256
Stadnytskyi, V., Bax, C.E., Bax, A., Anfinrud, P., 2020. The airborne lifetime of small speech droplets and their potential importance in SARS-CoV-2 transmission. Proceedings of the National Academy of Sciences 117, 11875–11877. https://doi.org/10.1073/pnas.2006874117
Sze To, G.N., Chao, C.Y.H., 2010. Review and comparison between the Wells–Riley and dose-response approaches to risk assessment of infectious respiratory diseases. Indoor Air 20, 2–16. https://doi.org/10.1111/j.1600-0668.2009.00621.x
Tang, J., Heinimann, H.R., 2019. Quantitative evaluation of consecutive resilience cycles in stock market performance: A systems-oriented approach. Physica A: Statistical Mechanics and its Applications 532, 121794. https://doi.org/10.1016/j.physa.2019.121794
Tao, F., Zhang, H., Liu, A., Nee, A.Y.C., 2019. Digital Twin in Industry: State-of-the-Art. IEEE Trans. Ind. Inf. 15, 2405–2415. https://doi.org/10.1109/TII.2018.2873186
Toner, G., 2008. Innovation, Science, Environment 08/09: Canadian Policies and Performance, 2008-2009. McGill-Queen's Press - MQUP.
van Doremalen, N., Bushmaker, T., Morris, D.H., Holbrook, M.G., Gamble, A., Williamson, B.N., Tamin, A., Harcourt, J.L., Thornburg, N.J., Gerber, S.I., Lloyd-Smith, J.O., de Wit, E., Munster, V.J., 2020. Aerosol and Surface Stability of SARS-CoV-2 as Compared

with SARS-CoV-1. New England Journal of Medicine 382, 1564–1567. https://doi.org/10.1056/NEJMc2004973
Villafruela, J.M., Olmedo, I., Berlanga, F.A., Ruiz de Adana, M., 2019. Assessment of displacement ventilation systems in airborne infection risk in hospital rooms. PLoS ONE 14, e0211390. https://doi.org/10.1371/journal.pone.0211390
Vuorinen, V., Aarnio, M., Alava, M., Alopaeus, V., Atanasova, N., Auvinen, M., Balasubramanian, N., Bordbar, H., Erästö, P., Grande, R., Hayward, N., Hellsten, A., Hostikka, S., Hokkanen, J., Kaario, O., Karvinen, A., Kivistö, I., Korhonen, M., Kosonen, R., Kuusela, J., Lestinen, S., Laurila, E., Nieminen, H.J., Peltonen, P., Pokki, J., Puisto, A., Råback, P., Salmenjoki, H., Sironen, T., Österberg, M., 2020. Modelling aerosol transport and virus exposure with numerical simulations in relation to SARS-CoV-2 transmission by inhalation indoors. Safety Science 130, 104866. https://doi.org/10.1016/j.ssci.2020.104866
Wang, C., Holmberg, S., Sadrizadeh, S., 2018. Numerical study of temperature-controlled airflow in comparison with turbulent mixing and laminar airflow for operating room ventilation. Building and Environment 144, 45–56. https://doi.org/10.1016/j.buildenv.2018.08.010
Wang, J., Huang, J., Feng, Z., Cao, S.-J., Haghighat, F., 2021. Occupant-density-detection based energy efficient ventilation system: Prevention of infection transmission. Energy and Buildings 240, 110883. https://doi.org/10.1016/j.enbuild.2021.110883
Wang, Z., Galea, E.R., Grandison, A., Ewer, J., Jia, F., 2022. A coupled Computational Fluid Dynamics and Wells-Riley model to predict COVID-19 infection probability for passengers on long-distance trains. Safety Science 147, 105572. https://doi.org/10.1016/j.ssci.2021.105572
Watanabe, T., Bartrand, T.A., Weir, M.H., Omura, T., Haas, C.N., 2010. Development of a Dose-Response Model for SARS Coronavirus. Risk Analysis 30, 1129–1138. https://doi.org/10.1111/j.1539-6924.2010.01427.x
Woelfel, R., Corman, V.M., Guggemos, W., Seilmaier, M., Zange, S., Mueller, M.A., Niemeyer, D., Vollmar, P., Rothe, C., Hoelscher, M., 2020. Clinical presentation and virological assessment of hospitalized cases of coronavirus disease 2019 in a travel-associated transmission cluster. MedRxiv 2020.
World Health Organization, 2021. Roadmap to improve and ensure good indoor ventilation in the context of COVID-19. World Health Organization, Geneva.
Yodo, N., Wang, P., 2016. Engineering Resilience Quantification and System Design Implications: A Literature Survey. Journal of Mechanical Design 138, 111408. https://doi.org/10.1115/1.4034223
Zhang, M., Shrestha, P., Liu, X., Turnaoglu, T., DeGraw, J., Schafer, D., Love, N., 2022. Computational fluid dynamics simulation of SARS-CoV-2 aerosol dispersion inside a grocery store. Building and Environment 209, 108652. https://doi.org/10.1016/j.buildenv.2021.108652
Zhu, S., Srebric, J., Spengler, J.D., Demokritou, P., 2012. An advanced numerical model for the assessment of airborne transmission of influenza in bus microenvironments. Building and Environment, International Workshop on Ventilation, Comfort, and Health in Transport Vehicles 47, 67–75. https://doi.org/10.1016/j.buildenv.2011.05.003
Zou, L., Ruan, F., Huang, M., Liang, L., Huang, H., Hong, Z., Yu, J., Kang, M., Song, Y., Xia, J., Guo, Q., Song, T., He, J., Yen, H.-L., Peiris, M., Wu, J., 2020. SARS-CoV-2 Viral

Load in Upper Respiratory Specimens of Infected Patients. New England Journal of Medicine 382, 1177–1179. https://doi.org/10.1056/NEJMc2001737